

Exotic $4f$ Correlated Electronic States of Ferromagnetic Kondo Lattice Compounds $ReRh_6Ge_4$ ($Re=Ce, Ho, Er, Tm$)

Yu Gao,¹ Jun Jiang,² Haiyan Lu,^{3,*} and Qiaoni Chen^{1,4,†}

¹*School of Physics and Astronomy, Beijing Normal University, Beijing 100875, China*

²*Computing Center Co. Ltd, Beijing Academy of Science and Technology, Beijing, 100094, China*

³*Science and Technology on Surface Physics and Chemistry Laboratory, P. O. Box 9-35, Jianguyou 621908, China*

⁴*Key Laboratory of Multiscale Spin Physics (Ministry of Education), Beijing Normal University, Beijing 100875, China*

CeRh₆Ge₄ stands out as the first stoichiometric metallic compound with a ferromagnetic quantum critical point, thereby garnering significant attention. Ferromagnetic Kondo lattice compounds $ReRh_6Ge_4$ ($Re=Ce, Ho, Er, Tm$) have been systematically investigated with density functional theory incorporating Coulomb interaction U and spin-orbital coupling. We determined the magnetic easy axis of CeRh₆Ge₄ is within the ab plane, which is in agreement with previous magnetization measurements conducted under external magnetic field and μ SR experiments. We also predicted the magnetic easy axes for the other three compounds. For TmRh₆Ge₄, the magnetic easy axis aligns along the c axis, thus preserving the C_3 rotational symmetry of the c axis. Especially, there are triply degenerate nodal points along the $\Gamma - A$ direction in the band structure including spin-orbital coupling. A possible localized to itinerant crossover is revealed as $4f$ electrons increase from CeRh₆Ge₄ to TmRh₆Ge₄. Specifically, the $4f$ electrons of TmRh₆Ge₄ contribute to the formation of a large Fermi surface, indicating their participation in the conduction process. Conversely, the $4f$ electrons in HoRh₆Ge₄, ErRh₆Ge₄ and CeRh₆Ge₄ remain localized, which result in smaller Fermi surfaces for these compounds. These theoretical investigations on electronic structure and magnetic properties shed deep insight into the unique nature of $4f$ electrons, providing critical predictions for subsequent experimental studies.

I. INTRODUCTION

Quantum criticality in heavy fermion materials has been a subject of ongoing experimental and theoretical research in the past twenty years. Heavy fermion materials usually contain lanthanides or actinides elements which involve partially filled f orbitals, so they are the typical strongly correlated electron systems. Abundant exotic phenomena have been intensively studied, such as unconventional superconductivity¹⁻⁴, non-Fermi liquid behaviors⁵⁻⁹, and exotic quantum critical phenomena¹⁰⁻¹². In some heavy fermion materials quantum criticality is largely driven by the competition between RKKY interaction and Kondo effect, and this mechanism falls in Landau's paradigm. However there is a large class of heavy fermion materials, on which the quantum critical point (QCP) is accompanied by the sudden breakdown of Kondo correlation. In the scenario of Kondo breakdown QCP, a jump occurs in the Fermi volume from large to small at the critical point. The Hertz-Millis-Moriya theory¹³⁻¹⁵ made foundation for the quantum critical phenomena of the itinerant fermions. In the ferromagnetic metallic materials, the ferromagnetic phase either enters into other ordered phase first, or enters into the paramagnetic phase through a first order phase transition¹⁶⁻²⁰. In the framework of Hertz-Millis-Moriya theory, two groups predicted that the ferromagnetic QCP is not stable in itinerant system^{17,21}. However recent experiments on CeRh₆Ge₄ show clear evidence of ferromagnetic QCP under high pressure²².

The germanide compound CeRh₆Ge₄ is a ferromagnetic metal, and it was synthesized from the elements

by Bisbuth fluxes²³. Resistivity measurements under high pressure²⁴ first suggest the existence of ferromagnetic QCP in CeRh₆Ge₄. Later detailed thermodynamic and transport measurements confirm the existence of the ferromagnetic QCP in CeRh₆Ge₄ under high pressure²². Then by silicon doping people also find ferromagnetic QCP²⁵ under chemical pressure. Although recent theoretical work suggests that if the material is noncentrosymmetric with strong spin-orbit coupling, is quasi-one-dimensional, or is sufficiently dirty, i.e., has a short electronic mean-free path, ferromagnetic QCP is possible to appear in itinerant electrons system²⁶. The nature of the ferromagnetic QCP on CeRh₆Ge₄ is still under debate. Whether it belong to the Kondo breakdown criticality^{22,27}, or there are two sequential effects near QCP as suggested by recent thermopower measurement²⁸. Recent numerical research indicates the anisotropy could lead to ferromagnetic QCP^{29,30}, meanwhile both angle-resolved photoemission spectroscopy (ARPES)³¹ and ultrafast³² optical experiments suggest the anisotropic hybridization of CeRh₆Ge₄.

Besides CeRh₆Ge₄ other isostructure compounds $ReRh_6Ge_4$, by substituting of Ce element into other lanthanides elements have been synthesized³³. At the same time they all have the LiCo₆P₄ type structure³⁴, and display rich exotic properties. Transport measurements indicate that along different direction the charge carriers of LaRh₆Ge₄ are with different type³⁵. La-doped CeRh₆Ge₄ display the crossover from coherent Kondo lattice behaviors to Kondo impurity regime³⁶. DFT calculations imply there are non-trivial topological properties in the band structure of YRh₆Ge₄, LaRh₆Ge₄

and LuRh_6Ge_4 ³⁷. Though YRh_6Ge_4 , LaRh_6Ge_4 and LuRh_6Ge_4 are non-magnetic, several other ReRh_6Ge_4 have local magnetic moments. Among them HoRh_6Ge_4 , ErRh_6Ge_4 and TmRh_6Ge_4 all have ferromagnetic ground state, same as CeRh_6Ge_4 . In this paper we perform the DFT calculations on the these four ferromagnetic germanide compounds. We first calculate the total ground state energy along different magnetic axes, and predict the easy axis of these compounds. Then we analysis the band structure, and find the nontrivial topological points in the band structure. In the end we calculate the DOS and Fermi surface, and find the evolution of the Fermi surface as the $4f$ electrons increases.

II. COMPUTATIONAL DETAILS

First-principles electronic structure calculations were performed using the fully potential (linear) augmented plane wave (FP-LAPW)+local orbital (lo) method implemented in the WIEN2k package^{38,39}. Exchange correlation functionals were performed using Perdew-Burke-Ernzerhof (PBE) type of generalized gradient approximation (GGA)⁴⁰. A $7 \times 7 \times 11$ k-points mesh is taken for the full Brillouin zone (BZ) sampling⁴¹, and the maximum cut of the wave vector was adjusted to $R_{min}^{mt} K_{max} = 8.5$. Murnaghan equation of state is utilized to obtain the zero temperature equilibrium structures. Once the equilibrium structures were obtained, the self-consistent calculations with an energy convergence value of 10^{-6} Ry and a charge convergence value of 10^{-4} were performed. Since the lathanides elements are heavy, the spin-orbital coupling (SOC) are considered. Due to the partially filled $4f$ orbital on the rare earth ions, the Hubbard U are also included in the calculations. So the SOC and Hubbard U are both included on the rare earth ions. Ferromagnetic calculations are performed for all of the four compounds, as they all have ferromagnetic ground state. However a knotty issue in the DFT calculations of the system with $4f$ electrons is that the energy curved surface can be complex. Sometimes the calculation are difficult to converge, and sometimes they get stuck in local minima⁴². To overcome these problems, we carefully chose the initial electronic configuration when searching for the ground state along different magnetic axes and the results are reliable.

III. RESULTS AND ANALYSIS

The lattice structure of the Kondo lattice compounds ReRh_6Ge_4 ($\text{Re}=\text{Ce}, \text{Ho}, \text{Er}, \text{Tm}$) belong to the hexagonal crystal system. The rare-earth ions forms triangular lattice in the ab plane, and the whole lattice are composed of a stack of triangular lattices along c axis as displayed in Fig. 1. The lattice constant along the c axis is much shorter than it along the a axis or b axis as shown in Table I. The ReRh_6Ge_4 lattice belong to the

TABLE I. Stable lattice parameters of the rare earth germanides ReRh_6Ge_4 ($\text{Re} = \text{Ce}, \text{Ho}, \text{Er}, \text{Tm}$).

Compound	$a / \text{\AA}$	$c / \text{\AA}$	a/c	Volume / \AA^3
CeRh_6Ge_4	7.201	3.881	1.855	174.282
HoRh_6Ge_4	7.236	3.840	1.884	174.124
ErRh_6Ge_4	7.239	3.836	1.887	174.087
TmRh_6Ge_4	7.238	3.836	1.886	174.039

non-centrosymmetric space group $P\bar{6}m2$, and is without space-inversion symmetry. As there are two kinds of inequivalent Rh ions and Ge ions, marked with light (dark) blue sites and light (dark) yellows sites in Fig. 1, the lattice is non-centrosymmetric. The first Brillouin zone is a hexagonal prism as displayed in Fig. 1 (c), the k_z direction is just along the c axis, the k_x direction is along the a axis, and the k_y direction is perpendicular to the k_x direction. The red points are the high symmetry points in the Brillouin zone. The distance of $\Gamma - A$ is longer since the c axis lattice constant is shorter.

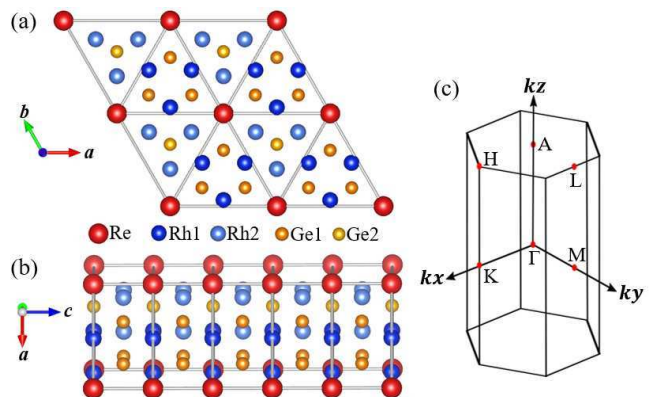


FIG. 1. (a) Top view and (b) perspective view along the c -axis of the crystal structure of ReRh_6Ge_4 ($\text{Re} = \text{Ce}, \text{Ho}, \text{Er}, \text{Tm}$). The red sites are rare-earth ions, and they form triangular lattice in the ab plane. The blue sites are Rh ions, and the yellow sites are Ge ions. (c) The first Brillouin zone of ReRh_6Ge_4 , and the red points are the high symmetry points.

The lattice constants of these Kondo lattice compounds ReRh_6Ge_4 are optimized by the Murnaghan equation of state⁴³ in the paramagnetic phase. The optimization start from the data of X-ray diffraction experiments on the powder samples³³, and our results are displayed in Table I. As the atomic number of rare-earth elements increases from CeRh_6Ge_4 to TmRh_6Ge_4 , the lattice constants along c axis become smaller, while the lattice constants along a axis tend to become bigger. The ratio of a/c becomes smaller, except from ErRh_6Ge_4 to TmRh_6Ge_4 . The volume of the unit cell becomes smaller as a result of the radius of the rare-earth ions decrease.

A. Ferromagnetic Ground State and Magnetic Easy Axis

Magnetic measurements indicates several rare-earth germanides are with local magnetic moments³³, such as GdRh_6Ge_4 , TbRh_6Ge_4 , DyRh_6Ge_4 and YbRh_6Ge_4 . Among them CeRh_6Ge_4 and the other three compounds we studied have ferromagnetic ground state. CeRh_6Ge_4 has been studied intensively, and its magnetic easy axis is within the ab plane according to the magnetization measurements²². The magnetic Bragg peaks is not resolved in neutron diffraction of powder sample, but the coherent oscillations are observed in zero-filed μSR measurements⁴⁴. The μSR measurements suggest the magnetic easy axis is along the a axis. In the following we implemented ferromagnetic DFT calculations to look for the magnetic easy axis. The spin-orbital coupling is included on Ce as it's a heavy element, and Hubbard U is fixed to 6 eV as previous work^{31,45}. Since lanthanides elements have unfilled $4f$ shells, the magnetism on these rare-earth germanides is mainly contributed by the lanthanides elements.

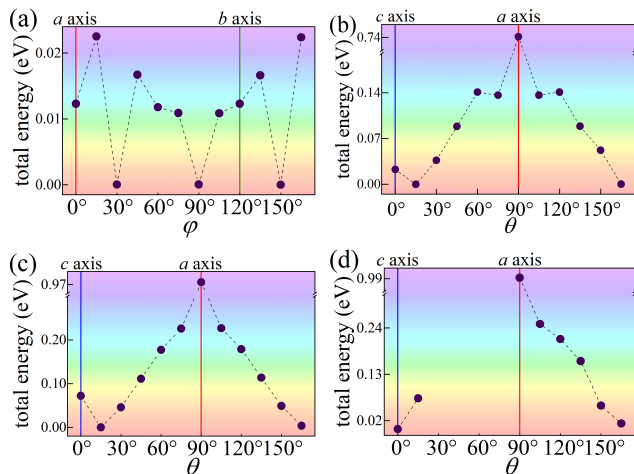


FIG. 2. The total ground state energy along different magnetic axis. (a) The ground state energy of CeRh_6Ge_4 when the magnetic axis is within the ab plane. φ is the angle with the a axis, so the red line and green line represent the a axis and the b axis respectively. (b)-(d) The ground state energy of HoRh_6Ge_4 , ErRh_6Ge_4 and TmRh_6Ge_4 when the magnetic axis is within the ac plane. θ is the angle with the c axis, so the blue line and the red line correspond to the c axis and the a axis, respectively.

We first calculate the ground state energy when the magnetic axis is along the lattice vector as shown in Table II. The total ground state energy is -1250481.63791 eV when the magnetic axis is along the c axis, while the total ground state energy is -1250481.70971 eV and -1250481.70971 eV along the a axis and b axis. When the magnetic axis is along the c axis the ground state energy is much higher, it indicates our calculations are in accordance with the experiments. The ground state

TABLE II. Ferromagnetic ground state energy of the rare earth germanides ReRh_6Ge_4 ($\text{Re} = \text{Ce}, \text{Ho}, \text{Er}, \text{Tm}$) along different axis.

Compound	a axis (eV)	b axis (eV)	c axis (eV)
CeRh_6Ge_4	-1250481.70971	-1250481.70971	-1250481.63791
HoRh_6Ge_4	-1352842.01992	-1352842.01993	-1352843.17190
ErRh_6Ge_4	-1365658.67112	-1365658.67112	-1365659.57456
TmRh_6Ge_4	-1378779.41052	-1378779.41052	-1378780.40282

the ab plane. The a axis is chosen as the x axis, thus the a axis correspond to $\varphi = 0^\circ$ and the b axis correspond to $\varphi = 120^\circ$. The ground state energy of CeRh_6Ge_4 is displayed in Fig. 2 (a), when the magnetic axis is within the ab plane. When $\varphi = 30^\circ$, $\varphi = 90^\circ$ and $\varphi = 150^\circ$, the ground state energy is the lowest. In Fig. 2 (a) the ground state energy subtract the ground state energy when $\varphi = 30^\circ$, and the value is -1250481.72198 eV. Thus our calculations imply the magnetic easy axis of CeRh_6Ge_4 is along $\varphi = 30^\circ$, $\varphi = 90^\circ$ and $\varphi = 150^\circ$.

The magnetization and susceptibility measurements³³ on HoRh_6Ge_4 , ErRh_6Ge_4 and TmRh_6Ge_4 indicate there are local magnetic moments on these compounds. The Curie temperature of HoRh_6Ge_4 and ErRh_6Ge_4 are all above zero, it suggests ferromagnetism on these two compounds. Both CeRh_6Ge_4 and TmRh_6Ge_4 have smaller local magnetic moment, so from the higher temperature magnetic measurements the Curie temperature is below zero. However recent experiments clarify the Curie temperature of CeRh_6Ge_4 is near 2.5K. The local magnetic moment of TmRh_6Ge_4 is larger than CeRh_6Ge_4 , thus the Curie temperature of TmRh_6Ge_4 should be higher than 2.5 K. Although the magnetic measurements are rare on HoRh_6Ge_4 , ErRh_6Ge_4 and TmRh_6Ge_4 , they all behave ferromagnetism. We have run the ferromagnetic DFT calculations on these three compounds. For TmRh_6Ge_4 , the total ground state energy is -1378780.40282 eV when the magnetic axis is along the c axis, smaller than -1378779.41052 eV and -1378779.41052 eV along the a axis and b axis. While for HoRh_6Ge_4 and ErRh_6Ge_4 , the total ground state energy along the c axis is also smaller than that along the a axis or b axis as shown in Table II. Thus be different from CeRh_6Ge_4 , the magnetic easy axis of the other three compounds is no longer within the ab plane. So we scan the ground state energy within the ac plane, and the results are shown in Fig. 2. The c axis is chosen as the z axis, thus the c axis correspond to $\theta = 0^\circ$ and the a axis correspond to $\theta = 90^\circ$, marked with blue line and red line respectively. On HoRh_6Ge_4 and ErRh_6Ge_4 the ground state energy is lowest when $\theta = 15^\circ$ and $\theta = 165^\circ$, while on TmRh_6Ge_4 the ground state energy is lowest when $\theta = 0^\circ$. When the magnetic axis is along $\theta = 15^\circ$ the ground state energy of HoRh_6Ge_4 and ErRh_6Ge_4 is -1352843.19446 eV and -1365659.64667 eV respectively, as are subtracted in Fig. 2(b) and 2(c). The ground state energy of TmRh_6Ge_4 is -1378780.40282 , when the magnetic axis

is along the c axis.

B. Band structure and potential topological properties

Previous DFT simulations on CeRh_6Ge_4 focus on the paramagnetic phase. We first perform the paramagnetic calculations and compare them with previous simulations, the band structure of our full potential full electron DFT calculations is consistent with these previous calculations. As the ferromagnetism play an important role in CeRh_6Ge_4 , here we mainly concentrate on the ferromagnetic calculations. The ground energy along different axis indicate the easy axis is along $\varphi = 30^\circ$, so we choose $\varphi = 30^\circ$ as the magnetic axis. The spin-orbit coupling can not be ignored on Ce , and neither the Hubbard U . If U is small the bands mainly contributed by $4f$ orbitals are quite close to the Fermi energy, and this is contradictory with the quantum oscillation experiment⁴⁵. In this paper we fix $U = 6 \text{ eV}$ following the previous simulations³¹. The band structure of CeRh_6Ge_4 are displayed in Fig. 3 (a) Several bands cross the Fermi energy, so CeRh_6Ge_4 is metallic as revealed by experiments. In order to see the contribution of the $4f$ electrons, the band structure is also projected to $4f$ orbitals. The $4f$ orbitals of the Ce^{3+} ions barely contribute to the bands near Fermi energy. As the electron configuration of Ce^{3+} is $4f^1$, the band constitute by $4f$ orbitals would be much lower than the Fermi level.

The band structure of HoRh_6Ge_4 and ErRh_6Ge_4 are displayed in Fig. 3 (b) and 3 (c). According to the band structure, both HoRh_6Ge_4 and ErRh_6Ge_4 are metals since several bands cross the Fermi level. The electron configuration of Ho^{3+} and Er^{3+} are $4f^{10}$ and $4f^{11}$. The blue dots in the figures indicate the contribution from $4f$ orbitals, and there are several bands near Fermi surface are constituted by $4f$ orbitals. There are also one band cross the Fermi level with blue dots covered, and that is due to the hybridization of $4f$ orbital and itinerant orbitals. The bands mainly constituted by $4f$ orbitals in ErRh_6Ge_4 is more close to Fermi energy compared with in HoRh_6Ge_4 . While in TmRh_6Ge_4 the situation is different as displayed in Fig. 3 (d). As the number of $4f$ electrons increasing, the bands close to Fermi energy have more contribution of $4f$ orbitals, and the valley near A point is lifted above Fermi level.

It is worth mentioning that the topological properties of the band structure. Due to the C_{3v} group symmetry along the c axis, and the space-inversion symmetry is not present in ReRh_6Ge_4 , there are triply degenerate nodal points in YRh_6Ge_4 , LaRh_6Ge_4 and LuRh_6Ge_4 ³⁷. If without SOC they all have two pairs of three fold degenerate points along the $\Gamma - A$ direction. The three-fold degenerate points are generated by the crossing of a non-degenerate band and a doubly degenerate band. When SOC is included the three-fold degenerate points changes to a pair of triply degenerate nodal points. A triply de-

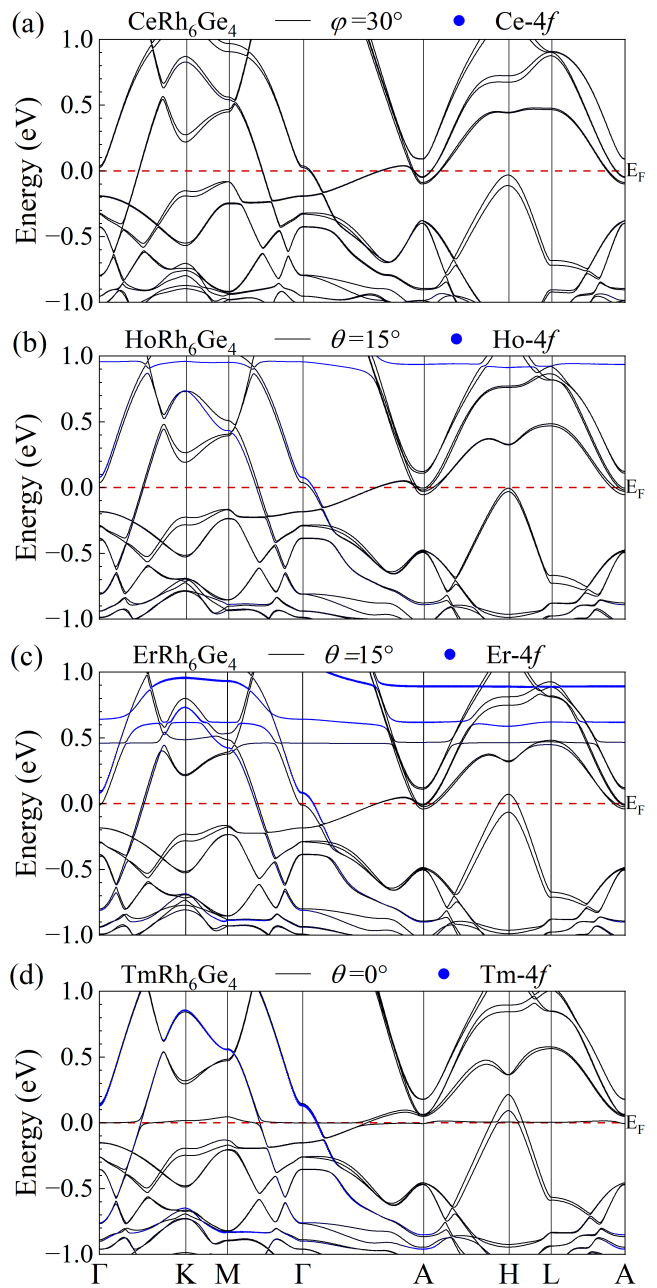


FIG. 3. Band structure of (a) CeRh_6Ge_4 , (b) HoRh_6Ge_4 , (c) ErRh_6Ge_4 and (d) TmRh_6Ge_4 along high symmetry paths in the BZ. The calculations are carried in the ferromagnetic phase with the SOC, and by fixed $U = 6 \text{ eV}$. These compounds are all metallic, with bands crossing the Fermi surface (red dashed lines). The blue lines are the Re - $4f$ orbital projected band structure.

generate nodal point is considered as intermediate state between double degenerate Weyl point and four-fold degenerate Dirac point. The C_{3v} group symmetry is kept in TmRh_6Ge_4 since the magnetic axis is along the c axis. There are also triply degenerate points in the band structure of TmRh_6Ge_4 along the $\Gamma - A$ direction. While in

CeRh₆Ge₄, HoRh₆Ge₄ and ErRh₆Ge₄ the the C_{3v} group symmetry is broken by the magnetic axis. The triply degenerate points disappear, leaving the Weyl points.

C. Density of states and Fermi surface

The density of states (DOS) of these compounds are shown in Fig. 4, and all the calculations are carried in the ferromagnetic case with SOC and $U = 6$ eV. Above and below the horizontal axis are the majority and minority components of the DOS. The partial DOS of different orbitals are displayed with different colors. Purple shaded areas represent the DOS of *Rh* 4*d* orbitals, orange lines represent the DOS of *Ge*-4*p* orbitals, and the blue lines represent the DOS of 4*f* orbitals. The total DOS (black lines in Fig. 4) is non-zero at Fermi energy, since these compounds are all metallic. The DOS around Fermi energy is mainly contributed by the 4*d* orbitals of *Rh* ions. As displayed in Fig. 4(a) there is a small blue peak near -2 eV below the Fermi energy of CeRh₆Ge₄. It represents the occupied 4*f*¹ state or the $J_{5/2}$ state considering SOC. While in HoRh₆Ge₄ and TmRh₆Ge₄ there are a few blue peaks above and close to the Fermi energy. They represent the unoccupied 4*f* orbitals. As more and more 4*f* orbitals are occupied from HoRh₆Ge₄ to TmRh₆Ge₄, one peak of the Tm-4*f* orbital is located at the Fermi energy. Thus the Tm-4*f* orbital is itinerant, and it contributes to the Fermi surface of TmRh₆Ge₄. As a result TmRh₆Ge₄ has a large Fermi surface, compared with the other three compounds on which 4*f* orbital is localized and the Fermi surface is small.

In order to shown the evolution of the Fermi surface volume, we simulate the Fermi surface of these compounds. The CeRh₆Ge₄ Fermi surface of our simulations are quite similar with previous results⁴⁵. There are eight bands cross the Fermi energy, so the Fermi surface of CeRh₆Ge₄ is composed by eight sheets. Four of them are hole type, and four of them are electron type. The Fermi surface of HoRh₆Ge₄ and ErRh₆Ge₄ are composed by eight sheets too, and four of them are electron type. Meanwhile the Fermi surface of TmRh₆Ge₄ is composed by six sheets, and only two of them are electron type. The cross session of the Fermi surface with the $k_x k_z$ plane displayed in Fig. 5, clearly shows the evolution of the Fermi surface. In TmRh₆Ge₄ the δ and δ' bands don't cross the Fermi energy, so the dark green and green lines are absent in Fig. 5 (d).

IV. SUMMARY AND OUTLOOK

Based on the empirical experimental evidence that the gemanides compounds $ReRh_6Ge_4$ ($Re=Ce, Ho, Er, Tm$) usually exhibit a ferromagnetic ground state, we have conducted the ferromagnetic DFT calculations on these compounds. By fixing the Coulomb interaction $U = 6$ eV and incorporating SOC effects, we predict the mag-

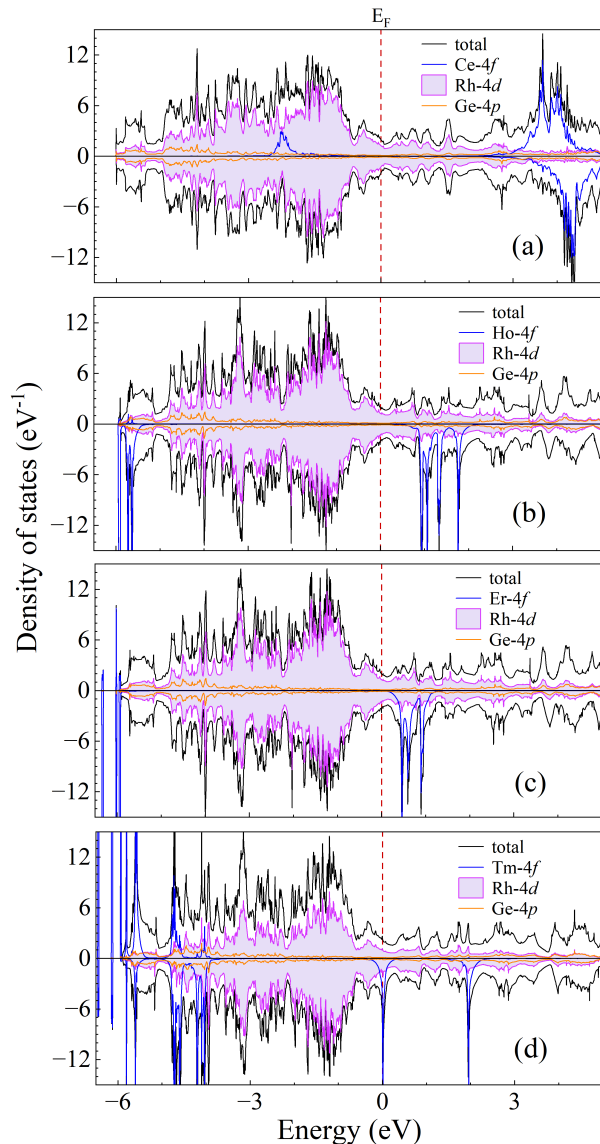


FIG. 4. Density of states of (a) CeRh₆Ge₄, (b) HoRh₆Ge₄, (c) ErRh₆Ge₄ and (d) TmRh₆Ge₄. The calculations are carried in the ferromagnetic phase with the SOC, and by fixing $U = 6$ eV. The total DOS is displayed with black line, and the partial DOS of *Ce*-4*f* orbitals, *Rh*-4*d* orbitals and *Ge*-4*p* orbitals are displayed with blue lines, shaped purple lines and orange lines.

netic easy axis of CeRh₆Ge₄ is within ab plane, with an angle of $\varphi = 30^\circ$ with respect to the a axis. For the less-explored compounds, our predictions reveal that HoRh₆Ge₄ and ErRh₆Ge₄ suggest their easy axis along the ac plane, with an angle $\theta = 15^\circ$ from the c axis. In contrast, TmRh₆Ge₄ possesses a magnetic easy axis aligned along the c axis, which preserves the C_{3v} point group symmetry. Intriguingly, within the $\Gamma - A$ direction, we observe the presence of triply degenerate nodal points in their band structures. The magnetic axes of the other three compounds, as a result of their unique mag-

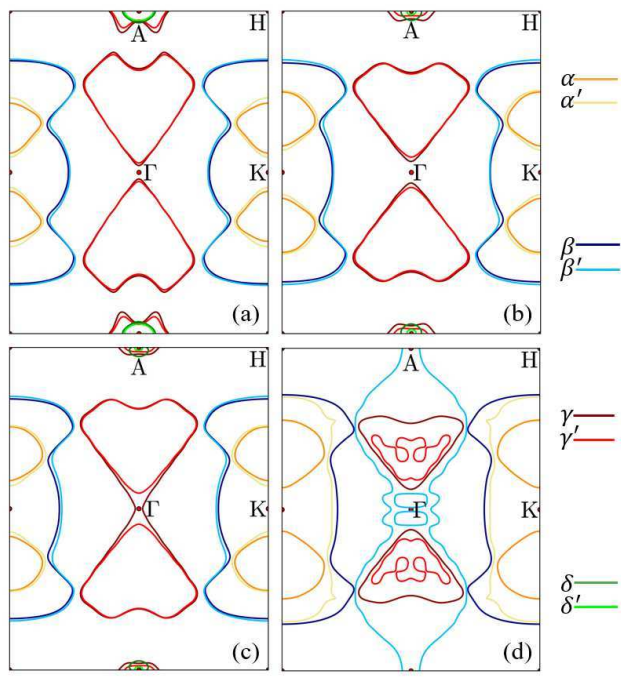


FIG. 5. The cross section of the xz plane and the Fermi surface of (a) CeRh_6Ge_4 , (b) HoRh_6Ge_4 , (c) ErRh_6Ge_4 and (d) TmRh_6Ge_4 calculated with the SOC and $U = 6 \text{ eV}$. The orange line (α), yellow line (α'), dark blue line (β) and blue line (β') represent the hole type bands, while the brown line (γ), red line (γ'), dark green line (δ) and green line (δ') represent the hole type bands.

netic properties, break the C_{3v} symmetry, even though

the nodal points are absent. Instead, Weyl points emerge along the $\Gamma - A$ direction. The density of states (DOS) analysis further elucidates the almost localized $4f$ states, and enhancing itinerancy of $4f$ states from HoRh_6Ge_4 to TmRh_6Ge_4 . TmRh_6Ge_4 boasts a substantial Fermi surface due to the active participation of the $4f$ electrons in its Fermi surface formation.

Recent thermoelectric measurements²⁸ reported an intriguing phenomenon in CeRh_6Ge_4 , where the onset of orbital-selective hybridization within the ferromagnetic phase at around 0.7 GPa leads to a discernible alteration in the Fermi surface geometry. Despite this, quantum oscillation data indicate that the extremal orbits on the Fermi surface remain unaltered across the critical temperature T_c . This discrepancy underscores the need for further numerical investigations on CeRh_6Ge_4 under pressure to delve deeper into the physics near the quantum critical point (QCP). Meanwhile, experimental studies on the isostructural counterparts, HoRh_6Ge_4 , ErRh_6Ge_4 and TmRh_6Ge_4 , remain relatively sparse. Our results shall establish a connection between magnetism and electronic structure, facilitating subsequent theoretical and experimental research.

ACKNOWLEDGMENTS

This work is supported by the National Science Foundation of China (Grant Nos.11974048, 11974049, 2022YFA1402201), CAEP Project (No. TCGH0710). We are grateful for the helpful discussions with Kai Liu and Pengjie Guo. We acknowledge National Super Computer Center in Tianjin for computing time.

* hyluphys@163.com

† qiaoni@bnu.edu.cn

¹ S. Ran, C. Eckberg, Q.-P. Ding, Y. Furukawa, T. Metz, S. R. Saha, I.-L. Liu, M. Zic, H. Kim, J. Paglione, and N. P. Butch, *Science* **365**, 684 (2019).

² L. Jiao, S. Howard, S. Ran, Z. Wang, J. O. Rodriguez, M. Sigrist, Z. Wang, N. P. Butch, and V. Madhavan, *Nature* **579**, 523 (2020).

³ Y. Y.-F. Li Yu, Sheng Yu-Tao, *Acta Phys. Sin.* **70**, 106 (2021).

⁴ J. Lin, *Physics* **49**, 586 (2020).

⁵ A. Legros, S. Benhabib, W. Tabis, F. Laliberté, M. Dion, M. Lizaire, B. Vignolle, D. Vignolles, H. Raffy, Z. Li, P. Auban-Senzier, N. Doiron-Leyraud, P. Fournier, D. Colson, L. Taillefer, and C. Proust, *Nature Physics* **15**, 142 (2019).

⁶ O. Trovarelli, C. Geibel, S. Mederle, C. Langhammer, F. M. Grosche, P. Gegenwart, M. Lang, G. Sparn, and F. Steglich, *Phys. Rev. Lett.* **85**, 626 (2000).

⁷ R. Daou, N. Doiron-Leyraud, D. LeBoeuf, S. Y. Li, F. Laliberté, O. Cyr-Choinière, Y. J. Jo, L. Balicas, J.-Q. Yan, J.-S. Zhou, J. B. Goodenough, and L. Taillefer, *Nature Physics* **5**, 31 (2008).

⁸ G. R. Stewart, *Rev. Mod. Phys.* **73**, 797 (2001).

⁹ H. v. Löhneysen, T. Pietrus, G. Portisch, H. G. Schlager, A. Schröder, M. Sieck, and T. Trappmann, *Phys. Rev. Lett.* **72**, 3262 (1994).

¹⁰ Q. Si and F. Steglich, *Science* **329**, 1161 (2010).

¹¹ C.-C. Liu, S. Paschen, and Q. Si, *Proc. Nat. Acad. Sci.* **120**, e2300903120 (2023).

¹² J. Custers, P. Gegenwart, H. Wilhelm, K. Neumaier, Y. Tokiwa, O. Trovarelli, C. Geibel, F. Steglich, C. Pépin, and P. Coleman, *Nature* **424**, 524 (2003).

¹³ J. A. Hertz, *Phys. Rev. B* **14**, 1165 (1976).

¹⁴ A. J. Millis, *Phys. Rev. B* **48**, 7183 (1993).

¹⁵ T. Moriya, *Spin fluctuations in Itinerant Electron Magnetism* (Springer, Berlin, 1985).

¹⁶ M. Brando, D. Belitz, F. M. Grosche, and T. R. Kirkpatrick, *Rev. Mod. Phys.* **88**, 025006 (2016).

¹⁷ D. Belitz, T. R. Kirkpatrick, and T. Vojta, *Phys. Rev. Lett.* **82**, 4707 (1999).

¹⁸ E. Lengyel, M. E. Macovei, A. Jesche, C. Krellner, C. Geibel, and M. Nicklas, *Phys. Rev. B* **91**, 035130 (2015).

¹⁹ V. Taufour, D. Aoki, G. Knebel, and J. Flouquet, *Phys. Rev. Lett.* **105**, 217201 (2010).

²⁰ M. Uhlarz, C. Pfleiderer, and S. M. Hayden, *Phys. Rev. Lett.* **93**, 256404 (2004).

- ²¹ A. V. Chubukov, C. Pépin, and J. Rech, *Phys. Rev. Lett.* **92**, 147003 (2004).
- ²² B. Shen, Y. Zhang, Y. Komijani, M. Nicklas, R. Borth, A. Wang, Y. Chen, Z. Nie, R. Li, X. Lu, H. Lee, M. Smidman, F. Steglich, P. Coleman, and H. Yuan, *Nature* **579**, 51 (2020).
- ²³ D. Voßwinkel, O. Niehaus, U. C. Rodewald, and R. Pöttgen, *Z. Naturforsch. B* **67**, 1241 (2012).
- ²⁴ H. Kotegawa, E. Matsuoka, T. Uga, M. Takemura, M. Manago, N. Chikuchi, H. Sugawara, H. Tou, and H. Harima, *J. Phys. Soc. Jpn.* **88**, 093702 (2019).
- ²⁵ Y. J. Zhang, Z. Y. Nie, R. Li, Y. C. Li, D. L. Yang, B. Shen, Y. Chen, F. Du, S. S. Luo, H. Su, R. Shi, S. Y. Wang, M. Nicklas, F. Steglich, M. Smidman, and H. Q. Yuan, *Phys. Rev. B* **106**, 054409 (2022).
- ²⁶ T. R. Kirkpatrick and D. Belitz, *Phys. Rev. Lett.* **124**, 147201 (2020).
- ²⁷ Y. Komijani and P. Coleman, *Phys. Rev. Lett.* **120**, 157206 (2018).
- ²⁸ S. M. Thomas, S. Seo, T. Asaba, F. Ronning, P. F. S. Rosa, E. D. Bauer, and J. D. Thompson, *Phys. Rev. B* **109**, L121105 (2024).
- ²⁹ J. Chen, J. Wang, D. Hu, and Y.-f. Yang, *Phys. Rev. B* **106**, 075114 (2022).
- ³⁰ J. Wang and Y.-F. Yang, *Sci. China-Phys. Mech. Astron.* **65**, 257211 (2022).
- ³¹ Y. Wu, Y. Zhang, F. Du, B. Shen, H. Zheng, Y. Fang, M. Smidman, C. Cao, F. Steglich, H. Yuan, J. D. Denlinger, and Y. Liu, *Phys. Rev. Lett.* **126**, 216406 (2021).
- ³² Y. H. Pei, Y. J. Zhang, Z. X. Wei, Y. X. Chen, K. Hu, Y.-f. Yang, H. Q. Yuan, and J. Qi, *Phys. Rev. B* **103**, L180409 (2021).
- ³³ D. Voßwinkel, O. Niehaus, and R. Pöttgen, *Z. Anorg. Allg. Chem.* **639**, 2623 (2013).
- ³⁴ R. Buschmann and H.-U. Schuster, *Z. Naturforsch. B* **46**, 699 (1991).
- ³⁵ S. Luo, F. Du, D. Su, Y. Zhang, J. Zhang, J. Xu, Y. Chen, C. Cao, M. Smidman, F. Steglich, and H. Yuan, *Phys. Rev. B* **108**, 195146 (2023).
- ³⁶ J.-C. Xu, H. Su, R. Kumar, S.-S. Luo, Z.-Y. Nie, A. Wang, F. Du, R. Li, M. Smidman, and H.-Q. Yuan, *Chin. Phys. Lett.* **38**, 087101 (2021).
- ³⁷ P.-J. Guo, H.-C. Yang, K. Liu, and Z.-Y. Lu, *Phys. Rev. B* **98**, 045134 (2018).
- ³⁸ P. Blaha, K. Schwarz, G. Madsen, D. Kvasnicka, and J. Luitz, *WIEN2k, An Augmented Plane Wave + Local Orbitals Program for Calculating Crystal Properties* (Karlheinz Schwarz, Techn. Universität Wien, Austria, 2001).
- ³⁹ G. K. H. Madsen, P. Blaha, K. Schwarz, E. Sjöstedt, and L. Nordström, *Phys. Rev. B* **64**, 195134 (2001).
- ⁴⁰ J. P. Perdew, K. Burke, and M. Ernzerhof, *Phys. Rev. Lett.* **77**, 3865 (1996).
- ⁴¹ P. E. Blöchl, O. Jepsen, and O. K. Andersen, *Phys. Rev. B* **49**, 16223 (1994).
- ⁴² B. Dorado, M. Freyss, B. Amadon, M. Bertolus, G. Jomard, and P. Garcia, *Journal of Physics: Condensed Matter* **25**, 333201 (2013).
- ⁴³ F. D. Murnaghan, *Proc. Nat. Acad. Sci.* **30**, 244 (1944).
- ⁴⁴ J. W. Shu, D. T. Adroja, A. D. Hillier, Y. J. Zhang, Y. X. Chen, B. Shen, F. Orlandi, H. C. Walker, Y. Liu, C. Cao, F. Steglich, H. Q. Yuan, and M. Smidman, *Phys. Rev. B* **104**, L140411 (2021).
- ⁴⁵ A. Wang, F. Du, Y. Zhang, D. Graf, B. Shen, Y. Chen, Y. Liu, M. Smidman, C. Cao, F. Steglich, and H. Yuan, *Science Bulletin* **66**, 1389 (2021).